



Full Text View

[Volume 28, Issue 2 \(February 1998\)](#)

Journal of Physical Oceanography

Article: pp. 178–190 | [Abstract](#) | [PDF \(228K\)](#)

Baroclinic Response of Sydney Shelf Waters to Local Wind and Deep Ocean Forcing

Mark T. Gibbs, Jason H. Middleton, and Patrick Marchesiello

School of Mathematics, University of New South Wales, Sydney, Australia

(Manuscript received August 8, 1996, in final form May 9, 1997)

DOI: 10.1175/1520-0485(1998)028<0178:BROSSW>2.0.CO;2

ABSTRACT

A study of the forcing processes responsible for upwelling events in the coastal ocean of Sydney, Australia, has been performed using data collected over the summer of 1994 from a shore-normal-aligned mooring array and a numerical model. Analyses of the data show that vertical displacements of fluid in the nearshore zone responded principally to the local wind stress during the experimental period. However, intrusions of mesoscale East Australian Current features are shown to significantly influence the vertical structure of the water column over the middle and outer shelf regions. Numerical simulations are performed to investigate the internal processes occurring during strong steady intrusion events of the East Australian Current onto the Sydney shelf. These simulations suggest that Ekman transport in the bottom boundary layer underlying an intrusion event is not an efficient mechanism for advecting colder water into the nearshore zone on the Sydney shelf. Preconditioning of shelf waters by the East Australian Current and concurrent forcing by local winds is suggested as an efficient process by which upwelling states may be achieved in the Sydney coastal ocean.

1. Introduction

In summer months, the coastal waters of Sydney, Australia, occasionally experience short periods of upwelling that significantly decrease the temperature (up to 8°C) of surface waters in the nearshore zone, defined here as the inshore 5 km of the shelf. The forcing processes responsible for these episodic events are not always evident. Local winds and the East Australian Current (EAC) can both play important roles in contrast to most other upwelling regions where local winds are the dominant upwelling forcing process.

Table of Contents:

- [Introduction](#)
- [Experimental program](#)
- [Salient features of the](#)
- [Magnitude of the upwelling](#)
- [Analysis of the data](#)
- [Numerical simulations](#)
- [Discussion](#)
- [REFERENCES](#)
- [APPENDIX](#)
- [TABLES](#)
- [FIGURES](#)

Options:

- [Create Reference](#)
- [Email this Article](#)
- [Add to MyArchive](#)
- [Search AMS Glossary](#)

Search CrossRef for:

- [Articles Citing This Article](#)

Search Google Scholar for:





- [Mark T. Gibbs](#)
- [Jason H. Middleton](#)
- [Patrick Marchesiello](#)


Only two previous studies of upwelling events on the Sydney coast have been undertaken. McClean-Padman and Padman (1991) used 10 years of weekly hydrographic data to determine the forcing processes behind upwelling events observed between 1972 and 1982. Most of the observed upwelling events coincided with either upwelling favorable local wind events or periods when mesoscale eddies shed from the EAC encroached onto the continental slope and shelf. [Griffin and Middleton \(1992\)](#) used data collected from an inshore mooring to analyze the response of the nearshore thermocline displacement to local and remote forcing. Results from this study indicated that local wind stress was the dominant forcing process for low-frequency (defined here as $<40^{-1}$ cph) baroclinic variability in the Sydney nearshore zone.

Analytical theories describing the barotropic response of continental margins to idealized wind and deep ocean forcing have been developed by [Csanady \(1978\)](#), [Middleton \(1987\)](#), and [Power et al. \(1990\)](#), among others. Analytical theories describing the baroclinic response of the coastal ocean to these forcing processes have been undertaken by [de Szoeke and Richman \(1983\)](#) and [Samelson and de Szoeke \(1988\)](#). Numerical techniques have also been used to investigate the response of shelf waters to upwelling forcing processes ([Allen et al. 1995](#)). These analytical and numerical studies have gone a long way toward elucidating the dynamics of wind-driven upwelling and upwelling forced by pressure gradients in the deep ocean; however, the role of the bottom boundary layer in particular is still not fully understood. Significant upwelling events observed on the New South Wales (NSW) continental shelf have been thought to be a result of EAC features intruding onto the shelf and slope (McClean-Padman and Padman 1991; [Cresswell 1994](#)) and one process by which these deep ocean currents are thought to force cooler waters into the nearshore zone is through the bottom boundary layer. The theory of [MacCready and Rhines \(1993\)](#), however, suggests that in idealized conditions the boundary layer may be shut down over the deeper continental slope.

The conflicting results from some of the studies of baroclinic processes in the NSW coastal ocean indicate that the roles of local wind and deep ocean forcing during upwelling and downwelling events on the NSW shelf remain unclear. The principle aim of this study is to investigate the dynamical behavior of the Sydney coastal ocean during several upwelling and downwelling events observed during the summer of 1994 and to seek relationships between the local wind and EAC forcing and the response of the coastal ocean.


2. Experimental program

The R.V. *Franklin* was used to deploy the current meter moorings and collect CTD data over the Sydney continental shelf ([Fig. 1](#) ) from the nearshore zone out to just beyond the shelf break ([Fig. 2](#) , [Table 1](#) ). This cruise commenced on 19 January 1994. The current meter moorings were recovered on 28 March 1994 and a second cruise aboard the R.V. *Franklin* commencing on 4 April was used to collect CTD data. Two additional moorings (A and C, [Fig. 2](#) ) containing thermistor strings were independently deployed prior to the first cruise and retrieved after the second.

The current meters were named according to their mooring location and position within the mooring: for example, F1 refers to the top current meter on mooring F, which was located farthest offshore. Mooring B is a permanent mooring that is often referred to as the Ocean Reference Station (ORS; [Griffin and Middleton 1991](#)) and that also possesses an anemometer that was used to collect the wind velocity data used in this study. Moorings A, B, and C contained thermistor strings that covered most of the water column in each case. Moorings D, E, and F contained current meters and those on moorings E and F also featured thermistors incorporated in the current meters. Mooring B also contains two current meters ([Table 1](#) ). The top current meters on moorings B, D, E, and F, designated as B1, D1, E1, and F1, were expected to remain within the surface mixed layer. Current meters B2, D3, E3, and F2 were expected to remain below the base of the mixed layer, which varied from around 40 m inshore to around 60 m over the slope for most of the experiment. Data recovery from the instruments was good with the exception of current meters F1 and F2, which returned data for 57 and 27 of the possible 63 days, respectively. For much of the experimental period, the high temperatures experienced in the nearshore zone exceeded the temperature range of the thermistor string on mooring A, and temperatures above the thermistor threshold of 23.4°C were truncated over approximately 30% of the experimental period.

The winds and currents were aligned with the principal alongshore and across-shore directions, which were obtained from the local bathymetry at each mooring site and deemed to be 11, 13, 17, and 29 degrees east of true north for moorings B, D, E, and F, respectively. A time series of wind stresses was then calculated from the wind velocity data using the formulation of [Large and Pond \(1981\)](#). The coastal aligned wind stresses and currents, along with the thermistor data, were then low-pass filtered to remove tidal, inertial, and other high-frequency signals using a Lanczos-cosine type filter with a cutoff period of 40 h.

3. Salient features of the data

Between days 1 and 26 several periods of prolonged southward winds occurred ([Fig. 3](#) ). The maximum strength of these upwelling favorable events was 0.13 Pa, in contrast to the strongest downwelling favorable wind event, which was 0.47 Pa in magnitude. Prolonged upwelling favorable wind events on the Sydney shelf are infrequent (McClean-Padman and Padman 1991), so we were fortunate to observe such events in this study.

The dominant feature in the currents was the strong southward flowing current event that occurred between days 24 and 37 (as highlighted in [Fig. 3](#)) during which the wind was predominantly in the opposite direction. Although these southward currents may be seen in the records from the inshore current meters, B1 and B2, the magnitude was greatest in the current meters located offshore ([Fig. 3](#)). Another strong southward current event may be seen in the currents from F1 at the start of the experimental period, and this event was only observed in the currents from F1 and E1 and was not observed over the inner shelf. The currents from F2 were northward during much of this period, highlighting the strong baroclinic structure of this event. Surface currents over the inner shelf were also northward during this period, which resulted in a strong horizontal current shear across the shelf. Southward currents coincided with southward upwelling favorable winds between days 3 to 26 and the magnitude of these currents decreased with distance offshore.

Strong northward currents at B1 between days 28–30 and 48–51 coincided with strong northward wind events. The alongshore current response to the first wind event is visible only in the data recovered from current meters B1 and B2, which were located in the nearshore zone; however, for the second event northward currents were recorded over the whole shelf. The currents from F1 between days 38 and 56 are also northward, and no corresponding strong wind event occurred until day 48 ([Fig. 3](#)). These northward currents did not penetrate onto the shelf prior to day 48; hence the shelf was insulated from this deep ocean event.

The low-passed temperature data from the thermistor string from mooring B and the thermistors incorporated into the current meters on mooring E may be seen in [Figs. 4](#) and [5](#). Upwelling (downwelling) events are represented by temperature minima (maxima) in these figures. The most dramatic features from the temperatures at B are the three periods of vertical homogenization commencing on days 27, 37, and 49 ([Fig. 4](#)), which coincided with periods of strong, northward winds ([Fig. 3](#)). The same events may be seen in the temperature data from the current meters on mooring E ([Fig. 5](#)). The temperatures at E3 show an increase in temperature of around 4°C for the first and third events but little change during the second period, which commenced on day 37. It is not possible from the temperature data alone to determine what proportion of the temperature changes are due to mixed layer deepening or direct advection onshore of warmer water during these downwelling events.

A broad, low-frequency upwelling period is evident at B and E between days 13 and 27 ([Figs. 4](#), [5](#)) when the wind stress was upwelling favorable ([Fig. 3](#)). This upwelling period ended with a strong homogenizing event on day 27 after which the two temperature plots do not follow the same trend. At B, the temperature stratification immediately reverts back to the state it was in prior to the homogenizing event ([Fig. 4](#)); however, at mooring E the temperature stratification did not revert back to the upwelled state ([Fig. 5](#)). There is also no evidence of a drop in temperature at the site of E4 between days 24 and 37 ([Fig. 5](#)) when the strong EAC currents were flowing over the shelf ([Fig. 3](#)). Such a drop in temperature at E4, which was positioned only 6 m above the seafloor, may have indicated active upwelling through the bottom boundary layer as a result of the strong upwelling favorable currents observed over the shelf and slope.

4. Magnitude of the upwelling and downwelling events

Estimates of vertical displacements over the shelf and inner slope were calculated to quantify the magnitude of the upwelling and downwelling events. Temperatures recorded by thermistors A10 (depth 45.0 m), B15 (depth 43.5 m), C7 (depth 44.9 m), and E3 (depth 46 m) were compared with a “background” temperature stratification ([Fig. 6](#)) to estimate the vertical displacement at different cross-shore locations. The background stratification was obtained by averaging the data from three shore-normal temperature sections acquired during a period of low EAC and local wind activity on the first cruise. This calculation assumed that the water retains its thermal properties during the vertical excursions. The thermistors chosen for the calculation were positioned just within the mixed layer for short periods during the experiment and the calculated displacements may be underestimates of their true values during these periods.

The estimates of the vertical displacements at the positions of moorings A and B were similar, and both of these moorings were positioned within one internal Rossby radius of the coast ([Figs. 7a,b](#)). The internal Rossby radius was calculated for all of the cross-shore density sections acquired from both cruises and found to be never less than 3 km from the coast. Similarly, the estimates of the vertical displacements at C and E, which were positioned more than one internal Rossby radius offshore from the coast, are similar ([Figs. 7c,d](#)). The displacements at the start and end of the experimental period were also nearly zero, indicating that the reference stratification chosen for the calculation was appropriate for the experimental period.

Between days 3 and 26, cooler waters were uplifted across the shelf and into the nearshore zone ([Figs. 7a,b](#)), and this coincided with the upwelling favorable winds that occurred during this period ([Fig. 3](#)). After day 13 the magnitudes of the estimates of the vertical displacements at moorings A and B increased to around 110 m; hence the fluid found at a depth of 45 m at mooring A had been upwelled through a vertical distance of 110 m, the source of which was around the shelf break at a depth of 155 m. No wind or deep ocean forcing event commenced on this day although both deep ocean forcing and local wind stress were upwelling favorable prior to day 13 ([Fig. 3](#)). The offshore migration of a coastal upwelled front past mooring B would result in such a decrease in temperature. Similar maxima occurred in the displacements at

moorings C and E on day 20 (Figs. 7c,d) although these peaks coincided with the strong deep ocean forcing (Fig. 3). The maximum displacement of 110 m demonstrates that only water from the outer shelf and upper slope was uplifted, and no deeper slope water was forced into the nearshore zone during the experimental period.

Three strong periods of downwelling, represented by displacement minima, were evident at nearshore moorings A and B, commencing on days 27, 36, and 48 (Fig. 7), and these events coincided with periods of downwelling favorable wind stress forcing (Fig. 3). Prior to the last downwelling event that commenced on day 48, the waters across the shelf were cooler (Figs. 4 and 5) and this coincided with strong, northward currents at F1 (Fig. 3), which are often associated with the intrusion of cold-core EAC features (Huyer et al. 1988). The intrusion of such a feature will reduce the temperature of the shelf waters and appear as a vertical displacement in Fig. 7.

5. Analysis of the data

The power density spectra of the unfiltered alongshore components of the wind stress and currents at F1, which is used as an estimate of the EAC, and the surface temperature at B1 were calculated (Fig. 8). The wind stress spectra shows a peak in the 10^{-2} to $10^{-2.6}$ cph band (~ 4 to 16 day period; defined here as the weather-band) and similar peaks are evident in the nearshore temperature spectra (Fig. 8). The spectra for the alongshore currents at F1 shows significant energy density levels for the low-frequency bands (10^{-3} cph and below); however, the unstationary nature of the EAC signal may have acted to spread energy across these low-frequency bands. Several peaks in the weather-band are also evident in this spectra, which may have been associated with local or remote wind-driven currents. The temperature spectra also exhibits significant energy density in the lower frequency bands.

The squared coherence and phase spectra between the two forcing functions and the nearshore surface temperatures were also calculated (Fig. 9). A strong relationship (squared coherence of 0.9) was found between the wind stress and temperatures at B1 in the weather-band (Fig. 9). In contrast the alongshore currents at F1 and the temperatures at B1 were incoherent with the exception of high coherences (0.8) centered at $10^{-2.5}$ cph (13 days) and higher than 10^{-2} cph (100 h). The squared coherence for frequencies lower than the weatherband were below the 95% confidence level.

Ekman theory was used to estimate the response of the nearshore temperature field to wind forcing alone. Ekman theory predicts that the cross-shore volume transport per unit length alongshore in the surface Ekman layer Q may be calculated from

$$Q = \frac{\tau^y}{\rho f}. \quad (1)$$

Here τ^y is the alongshore component (positive northward) of the wind stress, ρ is the mean density of the surface mixed layer, and f is the local value of the Coriolis parameter. If it is assumed that the vertical displacements of the base of the mixed layer η are confined to within an internal Rossby radius R_{oi} of the coast, then the averaged vertical velocity w of the interface of the mixed layer within an internal Rossby radius may be calculated from

$$w = \frac{\tau^y}{\rho f R_{oi}}. \quad (2)$$

A time series of vertical displacements of the base of the mixed layer η may be calculated for the hourly records of alongshore wind stresses by integrating the vertical velocities. These displacements can then be referenced against the background stratification used to calculate the vertical displacements (Fig. 6) to give a prediction of the isotherm response to the observed local wind forcing.

The solid line in Fig. 10 shows the temperatures measured by thermistor B13, located at a depth of 37.5 m on mooring B. The dashed line shows estimates of the temperatures at the same depth calculated by integrating the vertical velocities predicted from the offshore surface Ekman transport. For most of the experimental period the agreement between the observed and predicted temperatures shown is good (squared correlation coefficient of 0.95). Between days 18 and 26 and after day 50 the agreement is poor, which is probably a result of the intersection of the selected isotherms with the surface and bottom boundaries. The dashed line in Fig. 10 is meaningless during these periods. The only other period when the linear theory did not adequately predict the interfacial displacement is during the downwelling event between days 26 and 30 when the nearshore water column was fully homogenized (Fig. 4). This result is significant as it indicated that the nearshore thermocline displacement was primarily forced by the local wind stress, which agrees with the conclusions of Griffin and Middleton (1992) but is in contrast with the conclusions of McClean-Padman and Padman (1991).

An empirical orthogonal function analysis was performed on the alongshore and across-shore components of the low-

passed currents from E1 to E4 (Fig. 11). The first three EOF modes for the alongshore currents accounted for 94%, 4%, and 1% of the total variance for modes 1, 2, and 3 respectively, and together these lower modes accounted for 99% of the total variance. Similarly the first three EOF modes accounted for 98% of the total variance in across-shore currents (Fig. 11) with the first, second, and third modes individually accounting for 72%, 19%, and 7% respectively. The variance in both the across-shore and alongshore currents was dominated by flows that were in phase although at least 26% of the total variance in across-shore currents was accounted by flows exhibiting a reversal of the currents in the water column. This was probably a result of across-shore surface Ekman flows and interior and bottom return flows that occurred during wind driven upwelling and downwelling events. However, the EOF analysis does not give much insight into the time dependence of such interior and bottom boundary return flows and numerical techniques are required to answer such questions.

6. Numerical simulations

No evidence of direct upwelling resulting from the strong EAC intrusion event, which occurred between days 24 and 37, could be found, and this raises the question of the role of the EAC as an upwelling forcing process. Cresswell (1994) suggested that the EAC forces nutrient rich water onto the shelf through two processes. The first process involves a cyclonic, cold core eddy positioned between a mesoscale anticyclonic EAC eddy and the coast. This synoptic situation has been shown to advect cold deeper water into the shelf region (Huyer et al. 1988). Northward currents over the shelf and a net decrease in temperature of shelf waters are a consequence of the direct exchange of colder water over the shelf break during these EAC intrusion events (Figs. 3, 4, and 5 for days 47–53).

The second process by which the EAC may drive colder water up onto the shelf is through the cross-shore Ekman transport in the bottom boundary layer. These upwelling favorable bottom boundary layers are thought to be associated with warm core EAC features, which frequently encroach onto the continental slope of southeastern Australia (McCLean-Padman and Padman 1991). Hseuh and O'Brien (1971) developed an analytical barotropic model to show how a barotropic alongshore current may induce coastal upwelling. Boland (1979) suggested that this may be a process by which the EAC and its eddies produce upwelling on the NSW continental margin.

Allen et al. (1995) used a two-dimensional numerical model to simulate wind-driven upwelling events on the Oregon shelf. A similar model is used here to further investigate the role of the bottom boundary layer during strong EAC intrusion events. It must be stressed that the use of the numerical model here is not to attempt to simulate in detail the conditions observed during the experimental period. Rather, the model is used to clarify aspects of the physics for the case when a strong alongshore current flows over a narrow continental margin. Kelly and Chapman (1988), using a linear time-independent model incorporating an arbitrary bathymetry, found that the response of shelf waters to deep ocean forcing was weak and barotropic. In contrast, over the Sydney shelf the estimates of the interior displacements (Fig. 7) and vertical velocity shear observed in the currents (Fig. 3) demonstrate that the EAC intrusion events that occurred during the experimental period were strongly baroclinic over the outer shelf. This feature was also observed by Cresswell (1994).

The model was a two-dimensional (x, z) version of the Princeton Ocean Model (POM) that, unlike the model of Kelly and Chapman (1988), solves the full primitive equations (see Allen et al. 1995). The model was run using real bathymetry of the Sydney shelf and details of the configuration of the model are given in the appendix. Two numerical experiments were performed: the first experiment simulated a barotropic EAC intrusion event and the second experiment simulated a highly baroclinic EAC intrusion event. The experiments were designed to investigate the role of the bottom boundary layer on the shelf in upwelling scenarios driven by alongshore currents.

A steady barotropic jet was initially positioned over the shelf break for the first experiment (Fig. 12) and the maximum velocity in this jet was 0.7 m s^{-1} , which decreased linearly to a minimum value at the coast (see the appendix for details). The temperature field after day 1 shows that the bottom boundary layer is activated almost immediately (Fig. 12), as predicted by the theory of Hseuh and O'Brien (1971). Once the bottom boundary layer becomes established however, Ekman pumping out of the bottom boundary layer begins to tilt the isotherms up toward the coast in the interior, in particular beneath the center of the alongshore forcing jet. Adjustment of the alongshore velocity field to an approximate thermal wind balance results in a surface intensification of the alongshore velocities over the shelf and subsequently reduces the magnitude of the alongshore velocities directly above the bottom boundary layer. This reduction in the alongshore velocities toward the bottom of the water column acts to shut down the bottom boundary layer, beginning at the coast where the alongshore currents are weakest, and quickly moving out to the middle of the shelf. After fewer than 2 days, the bottom boundary layer in the nearshore zone is completely shut down.

The cause of the shutdown was not a result of the buoyancy effects investigated by MacCready and Rhines (1993). The one-dimensional theory of MacCready and Rhines (1993), which was developed for the case where flat isopycnals intersect a sloping bottom, showed how the buoyancy force created by the upslope transport of fluid in the bottom boundary layer acted to shut down the bottom boundary layer itself. In our case, it was the Ekman pumping out of the bottom boundary layer that acted to adjust the isopycnals in the interior above the bottom boundary layer, which subsequently introduced a strong vertical velocity shear in the alongshore component of the velocity. This reduction in the alongshore velocity

immediately above the bottom boundary layer damped before the “slippery bottom boundary layer” theory of [MacCready and Rhines \(1993\)](#) became important in the dynamical balance. Note that the shutdown process shown here is dynamically similar to that of [Chapman and Lentz \(1997\)](#)

The initial temperature field for the second experiment featured isotherms that tilted up toward the coast. The isotherm slope was 1%, which approximately matches the bottom slope and agrees with historical temperature sections ([Boland 1979](#)) and cross-shore temperature sections acquired during an EAC encroachment event on the Sydney shelf.

This condition introduces a baroclinic velocity component to the alongshore velocity field. The behavior of the bottom boundary layer during the second experiment ([Fig. 13](#)) is similar to the results obtained from the first experiment ([Fig. 12](#)). In both cases the thermal wind balance reduces the alongshore velocity directly above the bottom boundary layer in response to the tilting isotherms. For this second experiment the bottom boundary layer never became as deep as in the fast experiment and it actually took slightly longer to shut down over the shelf break.

The numerical simulations were repeated using different shelf bathymetries, both wider and narrower, and also with alternate stratifications obtained from the experimental program. The bottom boundary layer was found to shut down for these other model configurations.

The results from the numerical experiments suggest that the bottom boundary layer does not play an important role in driving upwelling during steady EAC intrusion events on the Sydney shelf. This does not mean that the EAC intrusion events do not contribute to upwelling in the nearshore zone. The upward tilting of the isotherms toward the coast as the EAC feature impinges over the shelf itself produces a horizontal temperature gradient across the shelf. Evidence of this may be seen in AVHRR sea surface temperature images presented in [Cresswell \(1994\)](#). It is, however, important to distinguish between the two processes. Nutrients advected across the shelf as a result of mass exchange as the isotherms are forced up inshore of the EAC eddy will travel along neutral surfaces. The path along which the nutrients pass in this process may be higher up in the water column than if the upwelling was occurring through the bottom boundary layer.

7. Discussion




Upwelling favorable winds occurred between days 3 and 26 of the experimental period and, although these winds were not strong, of the order of 0.1 Pa, the coastal ocean responded rapidly. Deeper shelf waters were uplifted through a vertical distance of around 35 m and transported into the nearshore zone by day 5 ([Fig. 7](#)). By day 15, cooler waters originating from the shelf break were found in the nearshore zone ([Fig. 7](#)) and a suspected coastal front had been advected offshore past the position of mooring B, located 3 km from the coast. Three strong downwelling favorable wind events also occurred during the experimental period. Commencing on days 26, 36, and 47 all three of these events fully homogenized the water column in the nearshore zone ([Fig. 4](#)), and a response to these events was observed in the temperature data from all the current meters on mooring E positioned just inshore of the shelf break ([Fig. 5](#)). Strong northward currents at mooring B were associated with these northward wind events commencing on days 27, 37, and 49 ([Fig. 3](#)).

The good agreement between the observed nearshore temperatures and those predicted by local wind forcing through Ekman dynamics ([Fig. 10](#)) clearly shows that the local wind stress was the dominant forcing process behind thermocline displacements in the nearshore zone. This conclusion is in agreement with the conclusions of [Griffin and Middleton \(1992\)](#). Although upwelling states on most continental shelves are produced by the action of the local wind stress, the importance of the local wind as an upwelling forcing process has perhaps been underestimated in other studies on the Sydney shelf and in some cases ignored.

Strong southward currents after day 24 at the positions of D, E, and F heralded the influence of an EAC eddy over the shelf, and no evidence of nearshore upwelling resulting from these strong currents was found ([Fig. 7](#)). The isotherms over the outer shelf tilted up toward the surface at the coast during this period as a result of the geostrophic balance; however, the strong northward wind event that commenced on day 27 reversed any currents driven by the EAC event in the nearshore zone and rapidly homogenized the water column. This result is significant as it shows how the currents resulting from strong EAC intrusion events can be quickly overwhelmed by local wind-driven currents in the nearshore zone on the Sydney shelf.

Between days 38 and 56, the currents at a depth of 44 m over the upper slope were northward; however, the local winds were southward until day 50 ([Fig. 3](#)). The isotherms over the shelf break were tilted down at the coast in a downwelling configuration, and the temperatures over the outer shelf decreased by 4°C ([Fig. 5](#)). The most plausible explanation for this temperature and velocity combination is the intrusion of a cold EAC feature similar to those observed by [Huyer et al. \(1988\)](#). The intrusion of such a feature cools the surface waters over the outer shelf first, unlike upwelling through the bottom boundary layer where surface cooling often commences at the coast.

[Tranter et al. \(1986\)](#) noted that many of the documented cases of nutrient enrichment of NSW shelf waters were

associated with features of the EAC. [Tranter et al. \(1986\)](#) also concluded that any dynamical links between coastal enrichment and the offshore EAC were not understood, although Ekman transport through the bottom boundary layer was thought to be the most likely mechanism ([Boland 1979](#)). The numerical EAC simulations ([Figs. 12](#) , [13](#) ) suggest that the bottom boundary layer does not play an important role in transporting cold, nutrient rich water into the nearshore zone during warm steady EAC intrusion events. The estimates of the vertical displacements from the observations during the EAC intrusion event between days 24 to 34 ([Fig. 7](#) ) also support this conclusion. However, this conclusion does not exclude EAC warm core eddies from contributing to upwelling forcing processes as transient EAC events may support upwelling favorable bottom boundary layers. The strong baroclinic structure of EAC intrusion events is evident from the large horizontal gradients presented in the temperature sections of the studies of [Huyer et al. \(1988\)](#) and [Boland \(1979\)](#). This tilting up of the isotherms toward the coast often results in outcropping of the isotherms, which takes on the appearance of an upwelling front. Some exchange of shelf and slope water must take place as the shelf waters adjust to the intrusion event and this is often confused with upwelling through the bottom boundary layer. The important difference between this adjustment process and wind-driven upwelling is that a continuous resupply of nutrient rich water occurs through the interior or boundary layer in the wind-driven case. In contrast, once the isotherms adjust to a EAC warm-core intrusion event, there is no steady-state process to continually force colder water up onto the continental shelf if the boundary layer is shut down. Baroclinic instability may also result in upwelling of colder nutrient rich waters in the vicinity of strong EAC features. Such parcels of water may then be advected along with the EAC feature. This may account for isolated parcels of colder water that have been observed along the NSW continental shelf (e.g., [Cresswell 1994](#)).

It is clear from the results shown in this study that, although the EAC was not the dominant forcing process behind variability in the nearshore zone during the experiment, the EAC did play an important part in determining the baroclinic structure over the outer shelf. It is also plausible that the EAC and local wind may act concurrently to produce active upwelling. Both warm EAC features and the local wind stress act to tilt the isotherms over the outer shelf and EAC events appear to “precondition” the shelf and slope waters, thereby enabling the local wind stress to more efficiently drive upwelling. We conclude that the most favorable conditions for upwelling on the Sydney shelf occur when the intrusion of a warm core EAC feature precedes a prolonged southward wind event. This may help to explain the conflicting conclusions drawn in previous studies of the upwelling on the Sydney shelf, which attempted to relate upwelling events to either local wind or EAC intrusion events but not both forcing processes acting concurrently.

Acknowledgments

The authors wish to thank the crew and scientific staff of the R.V. *Franklin* for their invaluable assistance in obtaining the data for this project and Greg Nippard of UNSW for his excellent technical support. This project was supported by the Australian Research Council Grant A39530680 and the Australian National Greenhouse Advisory Committee. Mark Gibbs was supported by an Australian Postgraduate Research Award during his Ph.D. candidature.

REFERENCES

- Allen, J. S., P. A. Newberger, and J. Federiuk, 1995: Upwelling circulation on the Oregon continental shelf. Part I: Response to idealized forcing. *J. Phys. Oceanogr.*, **25**, 1843–1866..
- Blumberg, A. F., and G. L. Mellor, 1987: A description of a three-dimensional coastal ocean circulation model. *Three-Dimensional Ocean Models*, N. Heaps, Ed., Amer. Geophys. Union..
- Boland, F. M., 1979: A time series of expendable bathythermograph sections across the East Australian Current. *Aust. J. Mar. Freshwater Res.*, **30**, 303–313..
- Chapman, D. C., and S. J. Lentz, 1997: Adjustment of stratified flow over a sloping bottom. *J. Phys. Oceanogr.*, **27**, 340–356..
- Church, J. A., H. J. Freeland, and R. L. Smith, 1986: Coastal-trapped waves on the east Australian continental shelf. Part I: Propagation of modes. *J. Phys. Oceanogr.*, **16**, 1929–1943..
- Cresswell, G. R., 1994: Nutrient enrichment of the Sydney continental shelf. *Aust. J. Mar. Freshwater Res.*, **45**, 677–691..
- Csanady, G. T., 1978: The arrested topographic wave. *J. Phys. Oceanogr.*, **8**, 47–62..
- de Szoeke, R. A., and J. G. Richman, 1984: On wind-driven mixed layers with strong horizontal gradients—A theory with application to coastal upwelling. *J. Phys. Oceanogr.*, **14**, 364–377..
- Griffin, D. A., and J. H. Middleton, 1991: Local and remote wind forcing of New South Wales inner shelf currents and sea level. *J. Phys. Oceanogr.*, **21**, 304–322..

- , and —, 1992: Upwelling and internal tides over the inner New South Wales continental shelf. *J. Geophys. Res.*, **97**, 14389–14405..
- Hseuh, Y., and J. J. O'Brien, 1971: Steady coastal upwelling induced by an along-shore current. *J. Phys. Oceanogr.*, **1**, 180–186..
- Huyer, A., R. L. Smith, P. J. Stabeno, J. A. Church, and N. J. White, 1988: Currents off southeastern Australia: Results from the Australian Coastal Experiment. *Aust. J. Mar. Freshwater Res.*, **30**, 245–288..
- Kelly, K. A., and D. C. Chapman, 1988: The response of stratified shelf and slope waters to steady offshore forcing. *J. Phys. Oceanogr.*, **18**, 906–925..
- Large, W. S., and S. Pond, 1981: Open ocean momentum flux measurements in moderate to strong winds. *J. Phys. Oceanogr.*, **11**, 324–336..
- MacCready, P., and P. B. Rhines, 1993: Slippery bottom boundary layers on a slope. *J. Phys. Oceanogr.*, **23**, 5–22..
- McCLean-Padman, J., and L. Padman, 1990: Summer upwelling on the Sydney inner continental shelf: The relative roles of local wind forcing and mesoscale eddy encroachment. *Contin. Shelf Res.*, **11**, 321–345..
- Middleton, J. H., 1987: Steady coastal circulation due to oceanic alongshore pressure gradients. *J. Phys. Oceanogr.*, **17**, 604–612..
- Power, S. B., R. H. J. Grimshaw, and J. H. Middleton, 1990: Large-scale, low-frequency barotropic circulation on continental margins. *J. Phys. Oceanogr.*, **20**, 769–785..
- Samelson, R. M., and R. A. de Szoeke, 1988: Semigeostrophic wind-driven thermocline upwelling at a coastal boundary. *J. Phys. Oceanogr.*, **18**, 1372–1383..
- Schahinger, R. B., and J. A. Church, 1994: The prediction of wind forced currents and sea level on the southeast Australian continental shelf. *J. Phys. Oceanogr.*, **24**, 2695–2702..
- Tranter, D. J., D. J. Carpenter, and G. S. Leech, 1986: The coastal enrichment effect of the East Australian Current eddy field. *Deep-Sea Res.*, **33**, 1705–1728..
-

APPENDIX

8. Numerical Model

The numerical simulations were performed using the Princeton Ocean Model. POM is a three-dimensional primitive equation ocean model that incorporates a turbulent closure scheme to provide realistic parameterization of the vertical processes. The model is described in detail in [Blumberg and Mellor \(1987\)](#), and for this study a simplified two-dimensional version of the model is used ([Allen et al. 1995](#)).

The width of the model domain is 50 km in the offshore direction and the maximum depth is 500 m. The vertical coordinate is terrain following, which implies a realistic representation of the bottom boundary layer and the influence of the bathymetry on the interior circulation. The vertical grid is composed of 50 levels, which are concentrated at the surface and bottom boundaries, and the horizontal grid spacing is 0.5 km. Increasing the vertical and across-shore resolution made no significant differences in the results from the simulations. The model bathymetry was obtained from charts and bathymetry data collected on the research cruises.

A large number of numerical experiments were performed to investigate the effect of an EAC intrusion event on the Sydney shelf, and two of these experiments are presented in [section 6](#). The initial conditions used in the two experiments were also constructed from data collected on the cruises. The temperature field was based on the profile shown in [Fig. 6](#) and for the first experiment the profile was extrapolated across the shelf. The initialization of a geostrophically balanced jet for the second experiment is as follows: First, the “background” stratification used in the first experiment was retained at the offshore boundary and an artificial isopycnal slope was introduced, the slope of which was chosen so that the isopycnals were approximately parallel to the bottom boundary. This matching of the isopycnals to the bottom slope is a characteristic commonly observed during EAC intrusion events, evidence of which may be seen in [Boland \(1979\)](#). The thermal wind relation was then used to calculate the baroclinic component of the currents. The barotropic component was obtained by imposing surface currents and a Gaussian jet was used to represent the cross-shore structure of the EAC intrusion event.

The domain is bounded offshore by a rigid wall, and to minimize the impact of this artificial boundary a relaxation term was added. No dynamical or thermodynamic forcing is imposed at the surface for these experiments; hence, the circulation evolves internally in response to the jet and bathymetry. The results were also averaged over an inertial period to attenuate

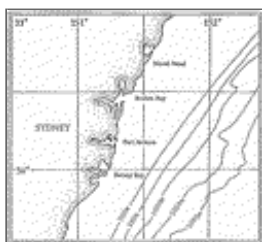
Tables

Table 1. Details of the current meter and thermistor string moorings deployed during the experiment. Note, unless otherwise explicitly stated, instruments refer to current meters.

Mooring name	Instrument ID	Instrument depth (m)	Water depth (m)
A	Thermistor string	11 thermistors between 17.7 and 45.0 m	50
B	Thermistor string	16 thermistors between 0.6 and 52.5 m	65
	B1	19.5	
C	B2	52.5	78
	Thermistor string	11 thermistors between 26.7 and 57.0 m	
D	D1	21.0	98
	D2	43.0	
	D3	65.0	
	D4	92.0	
E	E1	20.0	104
	E2	46.0	
	E3	72.0	
	E4	98.0	
F	F1	44.0	337
	F2	139.5	
	F3	330.0	

[Click on thumbnail for full-sized image.](#)

Figures



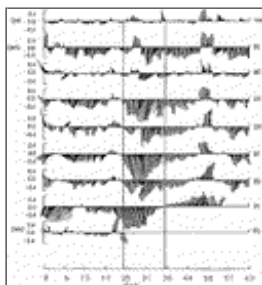
[Click on thumbnail for full-sized image.](#)

Fig. 1. Bathymetry of the Sydney shelf.



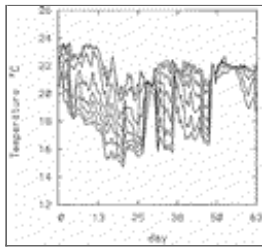
[Click on thumbnail for full-sized image.](#)

Fig. 2. Map of the Sydney shelf showing the positions of current meter and thermistor string moorings.



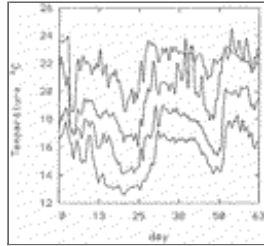
[Click on thumbnail for full-sized image.](#)

Fig. 3. Vector stick plots of the winds and currents. The top plot shows the wind stress. The names of the current meters are given on the right hand side of each plot. Oceanographic conventions are used throughout and the vector sticks are aligned to the principle alongshore and cross-shore directions.



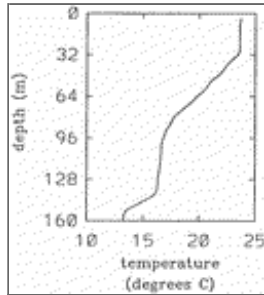
[Click on thumbnail for full-sized image.](#)

Fig. 4. Temperatures from the thermistor string on mooring B. Temperatures shown were measured at depths of 0.7, 2.7, 19.5, 22.5, 25.5, 31.5, 37.5, and 43.5 m. The total depth of the water-column at this site was 65 m.



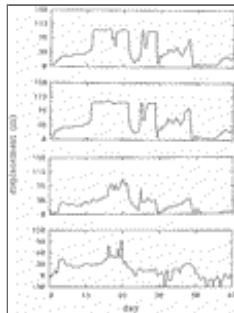
[Click on thumbnail for full-sized image.](#)

Fig. 5. Temperatures from current meters E1, E2, E3 and E4 positioned at depths of 20, 46, 72, and 92 m. The total depth of the water column at this site was 104 m.



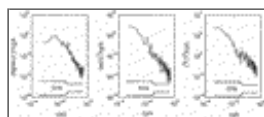
[Click on thumbnail for full-sized image.](#)

Fig. 6. Temperature profile acquired on 27 January 1994.



[Click on thumbnail for full-sized image.](#)

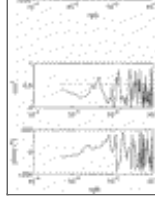
Fig. 7. Vertical displacements estimated from the temperature data at the position of moorings A, B, C, and E (panels a–d, respectively).



[Click on thumbnail for full-sized image.](#)

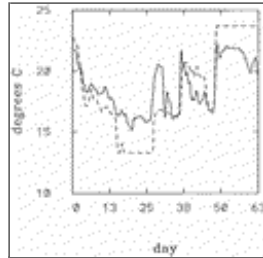
Fig. 8. Power density spectra of the wind stress (a), alongshore current (b) at F1, and temperature (c) at B1.





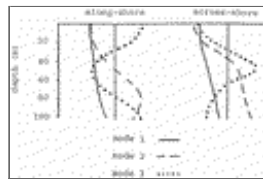
[Click on thumbnail for full-sized image.](#)

Fig. 9. Squared coherence and phase spectra (a: top pair) between the wind stress and temperature at B1 and (b: bottom pair) between the alongshore current at F1 and the temperature at B1.



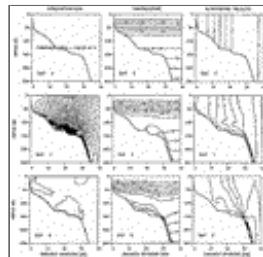
[Click on thumbnail for full-sized image.](#)

Fig. 10. Results from the surface Ekman transport calculation. The dashed line shows estimates of the temperatures at a depth of 37.5 m at mooring B, calculated by integrating the vertical velocities predicted from the offshore surface Ekman transport. The solid line shows the observed temperatures at this position.



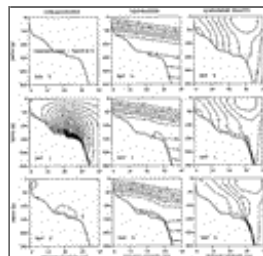
[Click on thumbnail for full-sized image.](#)

Fig. 11. First three empirical orthogonal function modes for the alongshore (a) and cross-shore (b) components of the currents at mooring E.



[Click on thumbnail for full-sized image.](#)

Fig. 12. Fields of the temperature T , the alongshore velocity \mathbf{U} , and the streamfunction for the cross-shore flow Ψ for the barotropic EAC experiment at days 0, 1, and 5. The contour intervals are: $\Delta T = 0.5^\circ\text{C}$; $\Delta \mathbf{U} = 0.05 \text{ m s}^{-1}$; and $\Delta \Psi = 0.1 \text{ m}^2 \text{ s}^{-1}$.



[Click on thumbnail for full-sized image.](#)

Fig. 13. As in [Fig. 12](#) but for the baroclinic EAC experiment.

top ▲



© 2008 American Meteorological Society [Privacy Policy and Disclaimer](#)
Headquarters: 45 Beacon Street Boston, MA 02108-3693
DC Office: 1120 G Street, NW, Suite 800 Washington DC, 20005-3826
amsinfo@ametsoc.org Phone: 617-227-2425 Fax: 617-742-8718
[Allen Press, Inc.](#) assists in the online publication of *AMS* journals.